RSC Advances

PAPER

Cite this: *RSC Adv.*, 2022, **12**, 15251

The formation mechanism of fibrous metal oxalate prepared by ammonia coordination method†

Huan Ma, Zhiyong Liu * and Zhihong Liu*

Anisotropic microstructures normally lead to different or better optical, electrical and magnetic properties for functional materials. We recently found some metal oxalates (nickel, cobalt, iron, silver, *etc.*) prepared in aqueous solutions will form fibrous morphology in the presence of ammonia (ammonia coordination method). Metals or metal oxides obtained by heating the fibrous metal oxalates in inert or oxidizing atmospheres can also inherit the high-aspect-ratio morphology. Ammonia coordination method is a simple and economical way to synthesize fibrous metal oxalates, metals, and metal oxides. In this work, fibrous nickel oxalate with a formula of $Ni(NH_3)_{1.7}C_2O_4 \cdot 2.2H_2O$ and its corresponding single crystal were synthesized to investigate the morphology transitions, structure transitions, and formation mechanism of fibrous particles. Ammonia molecules gradually coordinating with nickel atoms, which caused the increase of surface energy and atomic stacking rate of (020) crystal plane, was the fundamental reason for the oriented growth of nickel oxalate. Our results demonstrate a feasible method to synthesize high-aspect-ratio metallic materials and show the important influences of coordination ligand ammonia on the crystal growth stage of metallic materials which may provide references for synthesizing metallic materials with extraordinary microstructures and better properties by simple ammonia coordination method.

Received 28th January 2022
Accepted 29th April 2022

DOI: 10.1039/d2ra00605g

rsc.li/rsc-advances

1 Introduction

Metallic materials with high aspect ratios usually show good electrical conductivity, high catalytic efficiencies, and better electron transport properties due to their anisotropic microstructures and high surface areas.[1–5] Many methods, such as electrodeposition,[6,7] sol–gel,[8–10] surfactant mediated synthesis[11–14] and chemical etching,[15] have been developed to synthesize high-aspect-ratio nanoparticles.[16–18] However, these methods may not be suitable for large scale production mainly due to complex synthesis steps, expensive equipment and reagents, and operational difficulties. Our group found a simple one-step method to prepare nickel oxalate with fibrous micromorphology at atmospheric pressure which was just mixing the sodium oxalate solution and nickel chloride solution in the presence of ammonia (named as ammonia coordination method).[19,20] Heated in inert or oxidizing atmospheres, the fibrous nickel oxalate will decompose into nickel or nickel oxide which can succeed fibrous nickel oxalate's high-aspect-ratio morphology.[20,21] Other fibrous oxalates such as cobalt oxalate, iron oxalate, copper oxalate, silver oxalate, iron-nickel oxalate, and cobalt-nickel oxalate can also be synthesized by the ammonia coordination method.[22–27]

Through testing by a factory, the fibrous nickel prepared by the ammonia coordination-post calcination method showed equal or better performance in electrode additives and cemented carbide compared with nickel powders bought from the International Nickel Company. Quasi-one-dimensional $NiCo_2O_4$ synthesized through the ammonia coordination method also showed attractive microwave absorbing properties (reflection loss < 10 dB) in the frequency range of 6.82–18 GHz making it a promising candidate for electromagnetic wave absorber.[25] Fibrous nickel oxide (NiO) with a larger surface area of 140.153 $m^2\ g^{-1}$ and a lower electrical resistivity of $4.5 \times 10^5\ \Omega$ m had much better electrocatalytic activity than spherical NiO for ethanol oxidation.[28]

Ammonia coordination method is simple and economical for producing fibrous powder materials, however, there is little research on the formation mechanism of the fibrous particles. To better control the morphology of products and provide reference for synthesizing metallic particles with special morphology by simple coordination methods, the influences of critical experimental conditions, the transitions of nickel oxalate in feeding and aging processes, and the crystal structure of nickel ammine oxalate were investigated in this article.

2 Experimental

2.1 Materials

All chemical reagents were used as received without further purification. Nickel chloride hexahydrate ($NiCl_2 \cdot 6H_2O$), sodium oxalate ($Na_2C_2O_4$), ammonia solution 25–28% ($NH_3 \cdot H_2O$) and

School of Metallurgy and Environment, Central South University, Changsha, Hunan, 410083, PR China. E-mail: zhliu@csu.edu.com; csuliuzhiyong@163.com

† Electronic supplementary information (ESI) available. CCDC 2123391. For ESI and crystallographic data in CIF or other electronic format see https://doi.org/10.1039/d2ra00605g

polyvinylpyrrolidone K30 ($(C_6H_9NO)_n$) were obtained from Sinopharm (Shanghai, China). Deionized water was obtained from a laboratory purification system (>15.0 MΩ cm).

2.2 Preparation of fibrous nickel oxalate and chain-like nickel

In a typical synthesis experiment, 2.38 g of nickel chloride hexahydrate and 4.26 mL of ammonia solution (25–28%) were dissolved into 50 mL deionized water labelled as solution A. 1.34 g of sodium oxalate were dissolved into 50 mL deionized water giving solution B and 25 mL deionized water containing 0.31 g of polyvinylpyrrolidone K30 served as a substrate solution. The pH_{298K} values of the three as-prepared solutions were adjusted to 9.5 by hydrochloride and sodium hydroxide solutions. The substrate solution was put into a three-neck flask and heated to 80 °C in a water bath first. Then solution A and solution B were simultaneously pumped into the three-neck flask at a rate of 1 mL min^{-1} with continuously stirring at a speed of 200 rpm. The reaction system was kept at 80 °C for 4 h after pumping all the solutions for particle aging. The solid product and aqueous phase were separated by vacuum filtration followed by washing the solid product with DI water (×3) and ethanol (×3). Soft powders with a light blue color were obtained after drying the solid product in a vacuum drying oven at 25 °C for 24 h. The chain-like nickel was prepared by heating the fibrous nickel oxalate at 400 °C for 1 h in an argon atmosphere.

2.3 Synthesis of single crystal

Blue crystal $Ni(NH_3)_2C_2O_4$ was synthesized from a mixture of 0.1 g fibrous nickel oxalate prepared in the typical experiment conditions, 200 μL of 25–28% aqueous ammonia and 1 mL water, which was sealed in a 5 mL PTFE vessel and heated to 100 °C for 2 days, followed by cooling to 30 °C at 5 °C h^{-1}. To compare the structure difference of fibrous nickel oxalate and the blue single crystal, polycrystalline powders corresponding to the blue single crystal were synthesized by rotating the sealed PTFE vessel containing the same mixture at 100 °C for 6 h followed by cooling with the furnace, which would destroy the mild environment for the growth of single crystal.

2.4 Characterization

The morphology of samples was explored by a scanning electron microscope JEOL JSM-6360LV and a transmission electron microscope JEOL JEM-2100F. Powder X-ray diffraction (XRD) patterns were collected on a Rigaku TTR-III X-ray diffractometer with Cu Kα radiation ($\lambda = 0.15406$ nm). Bruker AXS Smart Apex II Single Crystal X-ray diffractometer was used to collect single crystal X-ray diffraction data. SHELX software was used to solve and refine the single crystral structure. Fourier transform infrared (FTIR) spectra of samples were recorded by a KBr pellet technique using a Thermo Fisher Nicolet 6700 spectrophotometer in the wavenumber range of 400–4000 cm^{-1}. The percentage composition of C, H, N elements present in samples was determined using an Elementar Vario EL III elemental analyzer. The contents of nickel in solid samples and reaction solutions were determined by ICP-AES instrument (ICP, Thermo Scientific, iCAP 7000). Thermogravimetric (TG) analysis was determined on Netzsch STA-449F3 TG/DTG instrument within a temperature range of 30 °C to 600 °C with a heating rate of 10 °C min^{-1} under an argon atmosphere.

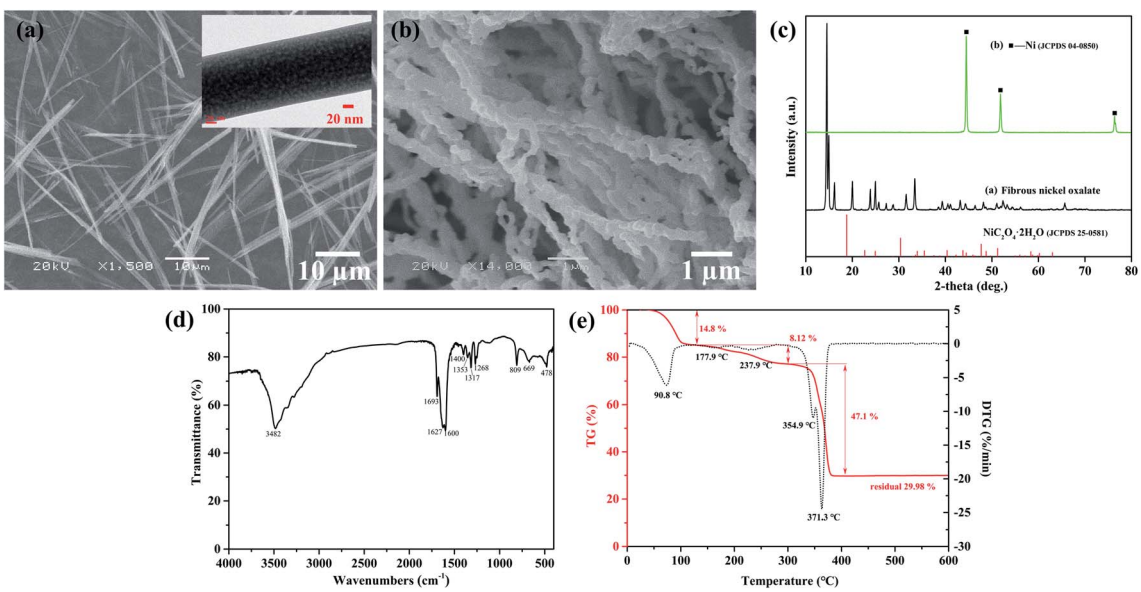

Fig. 1 Characterization of fibrous nickel oxalate. (a) SEM image of fibrous nickel oxalate prepared under the typical experiment conditions (inset shows high magnification TEM image of one nickel oxalate fiber). (b) SEM image of chain-like nickel after heating the fibrous nickel oxalate at 400 °C for 1 h in an argon atmosphere. (c) XRD patterns of the chain-like nickel (green line) and fibrous nickel oxalate (black line). (d) FTIR spectrum of the fibrous nickel oxalate. (e) Thermogravimetric (TG, solid line) and thermogravimetric derivative (DTG, dotted line) curves for the fibrous nickel oxalate.

3 Results and discussion

3.1 Characterization of fibrous nickel oxalate

The fibrous nickel oxalate with an average width of 0.29 μm and a length up to 87 μm were synthesized by the ammonia coordination method (Fig. 1a), while agglomerated nickel oxalate dihydrate particles presented without ammonia (Fig. S1a and b, ESI†). Some fibrous particles tended to agglomerate along their long axes due to the hydrophobicity of carbon atoms in oxalate. It was beneficial to lower the system energy if particles gathered and grew parallel with the direction of oxalate chains.[29] The XRD pattern of the fibrous nickel oxalate was totally different from nickel oxalate dihydrate and we did not find a standard JCPDS card consistent with it (Fig. 1c). After heating the fibrous nickel oxalate at 400 °C for 1 h in an argon atmosphere, the obtained nickel particles were chain-like also with high aspect ratios (Fig. 1b and c). The functional groups and modes of vibration from the FTIR spectrum of fibrous nickel oxalate were: 3482 cm^{-1}: $\nu_s(H_2O)$ + $\nu_s(NH_3)$, 1693 cm^{-1}: δ(HNH), 1627 cm^{-1}: ν_{as}(C═O), 1600 cm^{-1}: δ(HNH), 1400 cm^{-1}: $\rho(H_2O)$, 1353 cm^{-1}: ν_s(C–O), 1317 cm^{-1}: ν_s(C–O) + δ(O–C═O), 1268 cm^{-1}: ν_s(C–O), 809 cm^{-1}: ν_s(C–C), 669 cm^{-1}: δ(O–C═O), and 478 cm^{-1}: ν_s(Ni–O) (ν_s, ν_{as}, δ and ρ are stretching, symmetric stretching, bending, and wagging respectively) (Fig. 2d).[24,30,31] There were four molecular groups of crystallization water, –NH_3, Ni–O, and $C_2O_4^{2-}$ confirmed in the fibrous nickel oxalate based on the FTIR spectrum. The observed mass fraction of Ni, N, C and H in the fibrous nickel oxalate was 27.15 wt%, 11.04 wt%, 11.11 wt% and 4.44 wt% respectively, giving the molecular formula of fibrous nickel oxalate as $Ni(NH_3)_{1.7}C_2O_4 \cdot 2.2H_2O$. We attributed the non-integer of crystallization water and NH_3 in the molecular formula to the high reaction temperature at which some ammonia would be released from the product, and the relatively unstable crystal growth environment which would cause the fluctuation of the ammonia and water contents in every particle. There were two obvious endothermic peaks at 241.1 °C and 321.9 °C corresponding to the removal of crystalline water and decomposition of oxalate respectively in the TG-DTG curves of nickel oxalate dihydrate (Fig. S1c, ESI†).[32] Three obvious mass change stages of the fibrous nickel oxalate were found at temperature ranges of 25–110 °C, 110–300 °C and 300–400 °C (Fig. 1e). Based on the TG results, we heated the fibrous nickel

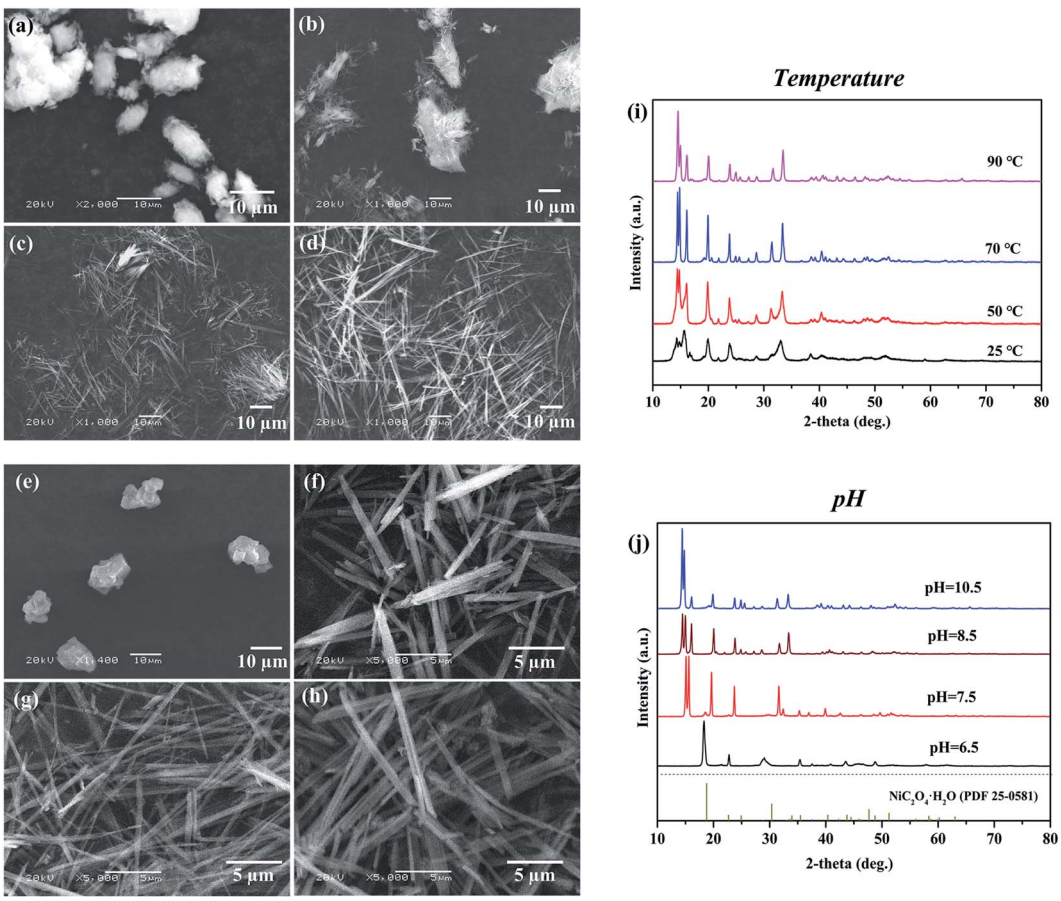

Fig. 2 The influence of temperature and pH on the morphology and crystal structure of nickel oxalate. (a–d) SEM images of nickel oxalate prepared at different temperatures: (a) 25 °C, (b) 50 °C, (c) 70 °C, and (d) 90 °C. (e–h) SEM images of nickel oxalate prepared at different pH of initial stock solutions: (e) 6.5, (f) 7.5, (g) 8.5, and (h) 10.5. (i) XRD patterns of nickel oxalate prepared at different reaction temperatures. (j) XRD patterns of nickel oxalate prepared at different pH. Only temperature or pH were changed in the above experiments while other experiment conditions were kept consistent with the typical experiment.

oxalate under an argon atmosphere at 110 °C and 300 °C for 1 h respectively to better understand its decomposition process. One endothermic peak appeared at 90.8 °C and the mass loss was 14.8% at the temperature range of 25–110 °C. According to the elemental analysis results for fibrous nickel oxalate after heating at 110 °C, the mass loss was mainly caused by the release of most NH_3 which in turn influenced the crystal structure of fibrous nickel oxalate, resulting in the decrease of crystallinity and XRD peak intensities though particles' morphology did not change a lot (Fig. S2a and c, ESI†). There existed two weak endothermic peaks at 177.9 °C and 237.9 °C with a mass loss of 8.12% in the temperature range of 110–300 °C. The particles after heating at 300 °C were still fibrous, of which most of nitrogen and hydrogen were eliminated with the carbon content unchanged (3.15 wt% of N and 1.19 wt% of H left after heating at 300 °C for 1 h) (Fig. S2b, ESI†). This indicated that most of the crystalline water and residual NH_3 were removed in this stage. The crystal structure of fibrous nickel oxalate was almost destroyed after losing NH_3 and crystalline water since many diffraction peaks disappeared in the XRD pattern (Fig. S2c, ESI†). With the continued elevation in temperature to 300–400 °C, there was a strong endothermic peak at 371.3 °C corresponding to the decomposition of oxalate. The relatively weak endothermic peak at 354.9 °C might be caused by the release of residual NH_3 and crystalline water leading to the mass loss (47.1%) a little higher than the theoretical value (40.89%) in the oxalate decomposition process. Finally, the fibrous nickel oxalate was transformed to chain-like nickel when the temperature was over 400 °C.

3.2 Key factors influencing the formation of fibrous nickel oxalate

The influence of reaction temperature, pH, Ni/NH_3 mole ratio, source of nickel ions, reactant concentration, feeding rate, surfactant, and stirring rate on the morphology of nickel oxalate had been investigated (Fig. S3, ESI†). We found the reaction temperature and pH were the two significant factors that made valuable contributions to the fibrous shape of nickel oxalate. Other factors affected the fibrous particle's length and width mainly by the degree of supersaturation. If the temperature and pH were set right, nickel oxalate with high aspect ratios could be synthesized regardless of the change of other factors.

When the reaction temperature was 25 °C keeping other conditions constant, the morphology of nickel oxalate became large bar-like with many tiny fibrous particles existing on its surfaces (Fig. 2a and S4a, ESI†). In a previous study, researchers proposed that high temperatures could modify the growth unit of nickel oxalate causing the growth rate of one crystal plane to become very fast which was the main reason for the fibrous shape of nickel oxalate prepared by the ammonia coordination method.[21] However, we found fibrous nickel oxalate also appeared after letting the collected aqueous phase after the solid–liquid separation in $T = 25$ °C experiment sealed in a plastic bottle at room temperature for several days, which suggested reaction temperatures controlled the morphology of nickel oxalate mainly by influencing the reaction rates (Fig. S4b, ESI†). At low temperatures, the reaction rates were relatively slow and the morphological transition of nickel oxalate to fibrous shape also needed a long time accordingly. The opinion was further confirmed by prolonging the aging time from 4 h to 9 h at the reaction temperature of 50 °C where the particles' morphology changed from agglomerations (Fig. 2b) to fibers (Fig. S4c, ESI†). When the reaction temperature was higher than 70 °C, nickel oxalate particles would be fibrous (Fig. 2c and d). We attributed the shorter length of fibrous particles at 70 °C than that of 90 °C to the higher reaction rates at 90 °C where the particles were more developed. The XRD patterns of nickel oxalate prepared at different temperatures were mostly similar except for the peaks at $2\theta = 12$–$18°$ (Fig. 2i). With the increase of temperature and length of particles, the peak at 12–18° would split into three peaks in which the intensity of the leftmost peak became the strongest suggesting the phase transformation occurred and the crystal plane corresponding to the leftmost peak was the predominant plane.

Then, the pH values of initial three solutions were changed simultaneously to study its influences on the formation of fibrous nickel oxalate. The nickel oxalate particles were granular when the solution pH was 6.5 and became rod-like at pH of 7.5 (Fig. 2e and f). In low pH conditions, ammonia NH_3 in the nickel-ammonia solution preferred to coordinate with H^+ forming ammonium ions NH_4^+.[33] The blue nickel-ammonia solution containing $Ni(NH_3)_n^{2+}$ ($n = 1$–6) would become green (the color of $Ni(H_2O)_6^{2+}$) when its pH was adjusted to 6.5 in our experiment. The lack of free ammonia at low pH caused the non-fibrous morphology of nickel oxalate particles. The XRD pattern of solid product at pH of 6.5 was a little different from nickel oxalate dihydrate which might be caused by the lattice distortion resulting from little ammonia incorporated in the crystal lattice of nickel oxalate. As more ammonia NH_3 existed at high pH, a new phase appeared when the pH was 7.5 and we also did not find a standard JCPDS card consistent with its XRD pattern (Fig. 2j). When the pH values were higher than 8.5, fibrous particles formed and their XRD patterns were similar to typical fibrous nickel oxalate (Fig. 2g, h and j).

3.3 Morphology and structure transition in feeding process

Samples including solid products and liquid phases were collected at different time during the synthesis of fibrous nickel oxalate. In the feeding process, large lump particles started to form first at the feeding time of 2 min (Fig. 3a) and then the lump particles were subsequently *in situ* disassembled into small spindle-like clusters (Fig. 3b). The small spindle-like particles grew into coarse separated columnar particles at 10 min (Fig. 3c) while fibrous particles appeared on their surfaces at 15 min (Fig. 3d) and the columnar particle began disintegrating from its two ends to many fibers at 20 min (Fig. 3e). In the meanwhile, the surface energy of particles increased with the rise of specific surface areas leading to the spontaneous re-agglomeration of columnar particles.[34] When the time was over 25 min, the columnar particles in the large clusters were progressively transformed to fibers and further the fibrous particles grew longer (Fig. 3f–k).

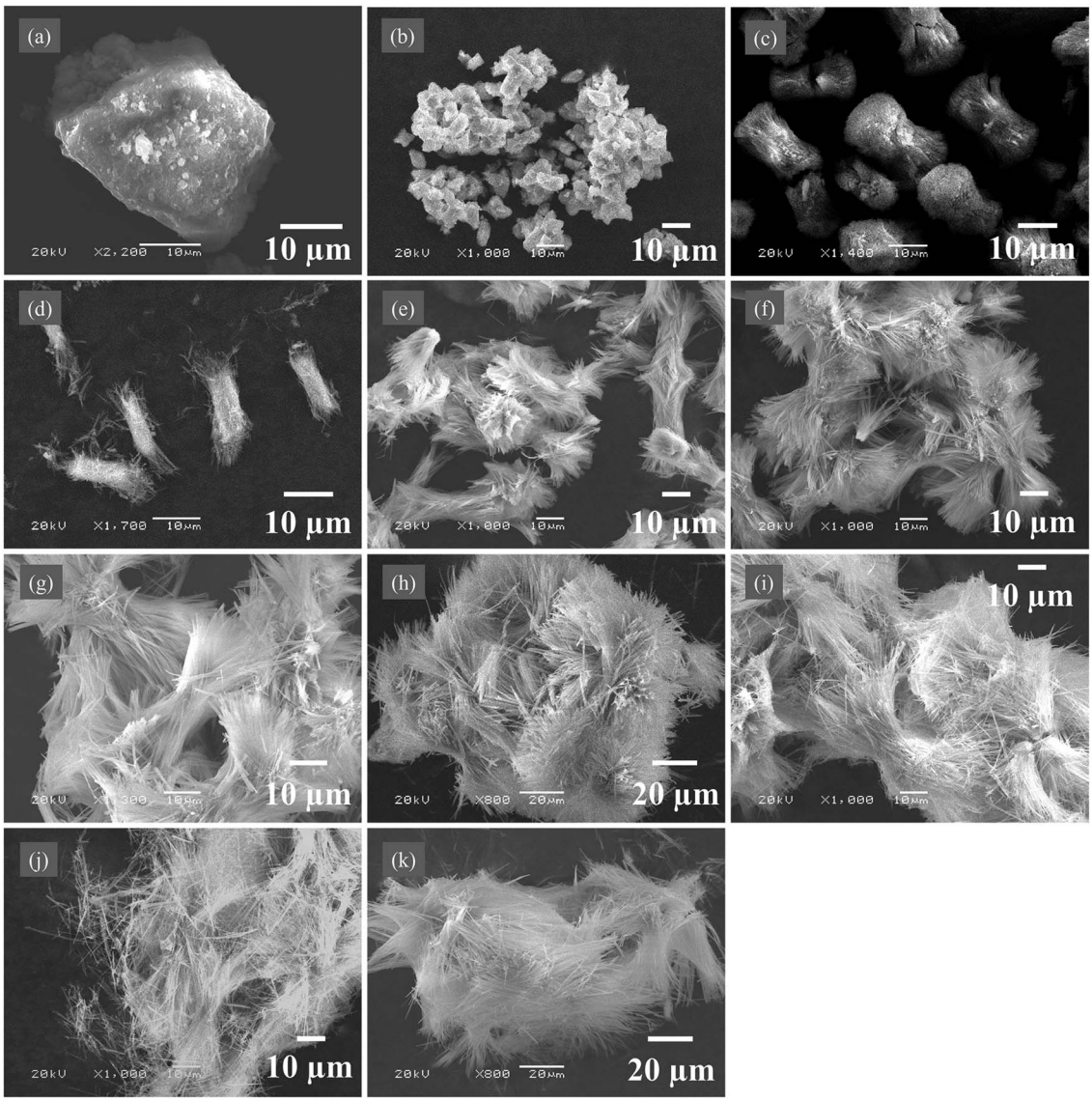

Fig. 3 The morphology transition of nickel oxalate prepared by the ammonia coordination method in the feeding process. SEM images show the morphology of nickel oxalate at different feeding time: (a) 2 min; (b) 5 min; (c) 10 min; (d) 15 min; (e) 20 min; (f) 25 min; (g) 30 min; (h) 35 min; (i) 40 min; (j) 45 min; (k) 50 min.

There were only crystalline water ($\nu_s(H_2O)$ at 3448.12 cm^{-1}), Ni–O (ν_s(Ni–O) at 478.59 cm^{-1}), and $C_2O_4^{2-}$ (ν_{as}(C=O) at 1628.73 cm^{-1}, ν_s(C–O) at 1316.25 cm^{-1}, ν_s(C–O) at 809.93 cm^{-1}, and ν_s(C–C) at 669.43 cm^{-1}) vibration peaks in the FTIR spectrum of solid product at the feeding time of 2 min, suggesting the initial precipitate was only composed of nickel ion Ni^{2+}, oxalate ion $C_2O_4^{2-}$ and crystalline water (Fig. 4a). When the feeding time exceeded 5 min, the characteristic peaks of NH_3 (δ(HNH) at 1692.09 cm^{-1} and 1597.65 cm^{-1}) appeared in the solid products and the peak at 3448.12 cm^{-1} shifted to the left due to the existence of ammonia. The nitrogen contents in solid products also increased from 6.32 wt% at 5 min to 10.73 wt% at 50 min (Fig. 4b). Taken together, these results indicated ammonia enter the crystal lattice of nickel oxalate incrementally though the most ammonia existed in the form of $Ni(NH_3)_n^{2+}$ (n = 1–6) in the initial nickel-ammonia solutions. The reaction equations were summarized as follows.

$$Ni(NH_3)_n^{2+} \rightarrow Ni^{2+} + nNH_3 \ (n = 1\text{–}6)$$

$$Ni^{2+} + C_2O_4^{2-} + xH_2O \rightarrow NiC_2O_4 \cdot xH_2O \ (2 \leq x < 3)$$

$$NiC_2O_4 \cdot xH_2O + yNH_3 \rightarrow Ni(NH_3)_yC_2O_4 \cdot xH_2O \ (0 < y \leq 2)$$

There were no diffraction peaks in the XRD pattern of solid product at 2 min indicating the initial product was an amorphous solid (Fig. 4c). As the incorporation of ammonia into the crystal lattice of nickel oxalate, atoms began orderly arranging to form solid products with weak crystallinity and diffraction peaks at 5 min. Accordingly, the morphology of nickel oxalate was transformed to small spindle-like clusters from lump particles

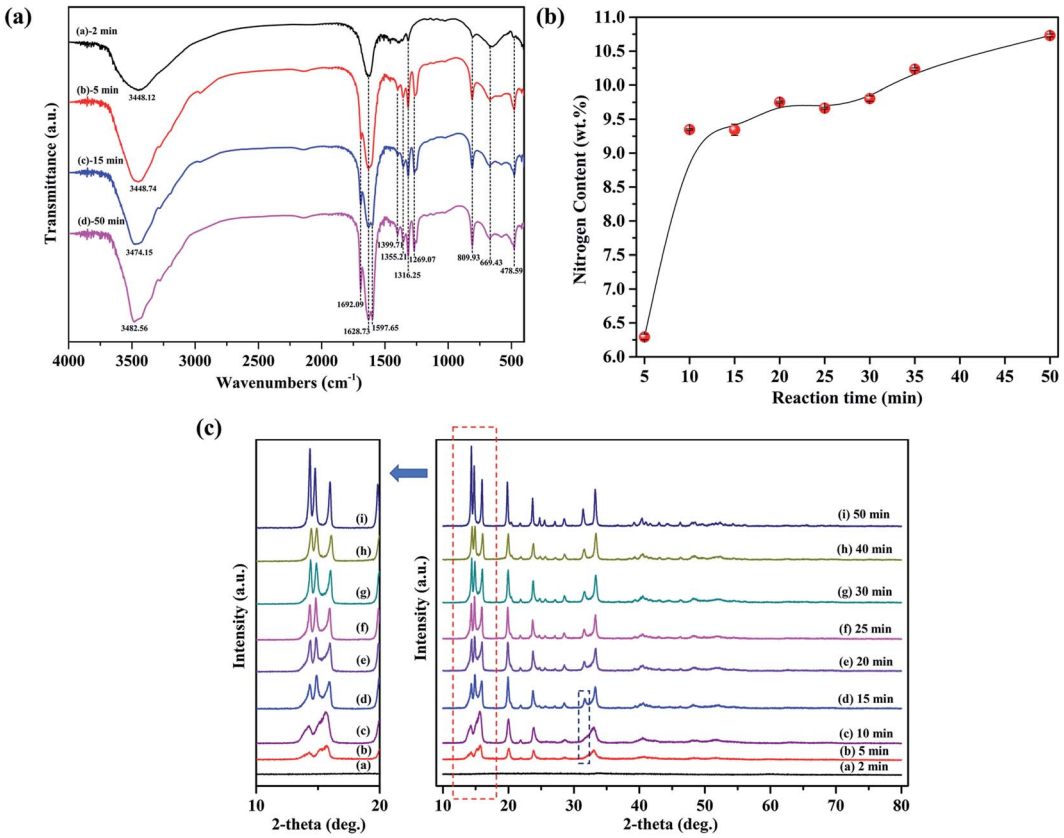

Fig. 4 The crystal structure transition of nickel oxalate prepared by the ammonia coordination method in the feeding process. (a) FTIR spectra of solid products obtained at different time during the feeding process. (b) Plot shows the nitrogen contents in solid products during the feeding process. (c) XRD patterns of solid products during the feeding process.

due to the change of crystal structure. The crystallinity of solid products at 10 min became better. The XRD pattern of solid products at 15 min showed that the two diffraction peaks at $2\theta =$ 10–20° split into three peaks and a new peak appeared at around 32° which indicated the crystal structure of nickel oxalate changed again causing the emergence of fibrous particles and the

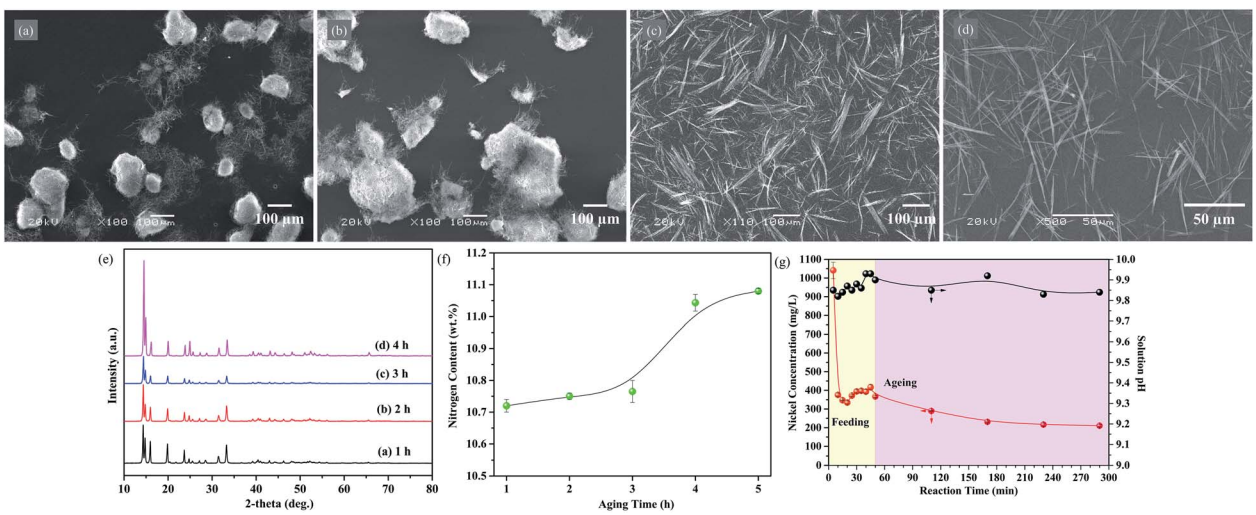

Fig. 5 The morphology and structure transition of nickel oxalate prepared by the ammonia coordination method in the aging process. (a–d) SEM images of nickel oxalate at different aging time: (a) 1 h; (b) 2 h; (c) 3 h; (d) 4 h. (e) XRD patterns of solid products obtained at different time during the aging process. (f) Plot shows the nitrogen contents in solid products during the aging process. (g) Plot shows the changes of nickel concentration and pH with time in the reaction solutions during the whole process.

disassembly of columnar particles. After 20 min, the position of XRD peaks kept constant while the crystallinity of solid products was gradually enhanced. The reaction system with low supersaturation switched to the crystal growth stage immediately after primary nucleation, which was in accordance with the LaMer model.[35]

3.4 Morphology and structure transition in aging process

The products were left in the reaction system for further 4 h to finish the evolution of fibrous particles after the feeding process. Large clusters consisting of tiny fibers still existed in the reaction system when the aging time was 1 h and 2 h (Fig. 5a and b). The clusters disappeared and became aggregated fibrous particles if prolonging the aging time to 3 h (Fig. 5c). At the aging time of 4 h, the nickel oxalate fibers became longer and well-dispersed compared with particles at 3 h (Fig. 5d). Ostwald ripening might occur during the aging process where thermodynamically unfavorable tiny fibrous particles dissolved to release chemical fuels for the growth of large fibrous particles. The disappearance of large clusters might be caused by the dissolution of small fibrous particles.

The nitrogen content of solid products increased slightly with the extension of aging time and became steady after 4 h (Fig. 5f). The X-ray diffraction peak positions at different aging time were consistent with the typical experiment product while the intensity of the leftmost peak rose faster than other peaks,

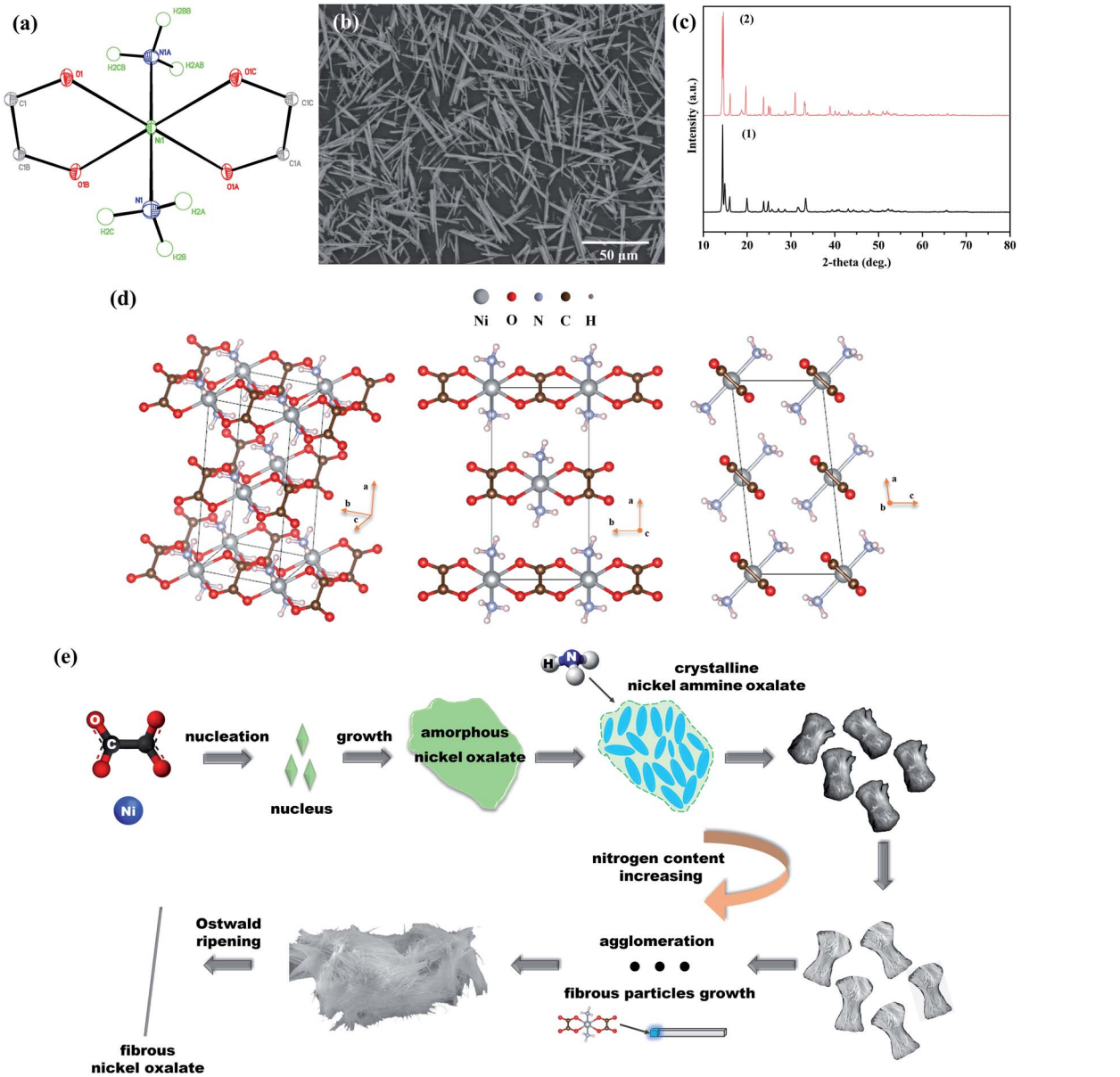

Fig. 6 The crystal structure of nickel ammine oxalate. (a) The coordination environment of nickel atom in $Ni(NH_3)_2C_2O_4$. (b) SEM image of the polycrystalline powders corresponding to $Ni(NH_3)_2C_2O_4$. (c) XRD patterns of the polycrystalline powders corresponding to $Ni(NH_3)_2C_2O_4$ (2) and the fibrous nickel oxalate (1). (d) View of the three-dimensional structure of $Ni(NH_3)_2C_2O_4$. (e) The formation process of fibrous nickel oxalate.

suggesting the crystal plane corresponding to the peak was gradually exposed as the growth of fibrous particles again (Fig. 5e).

The nickel ion concentration in the reaction solution dropped dramatically from 1041 mg mL^{-1} at 5 min to 375.6 mg mL^{-1} at 10 min, furthermore, the nitrogen contents in the solid products increased dramatically during this period indicating the quick transformation from spindle-like particles into columnar particles once ammonia was present in the crystal lattice of nickel oxalate (Fig. 5g). The nickel ion concentration decreased to 334.6 mg mL^{-1} at 20 min, but it would then begin to gradually increase until 45 min. As the time increased, the volume of reaction solutions in the three-neck flask continuously grew leading to the increase effect of nickel concentration through pumping feeding solutions becoming weak. Moreover, after 20 min, the consumption of nickel ions was dominated by the growth of fibrous particles where the consumption rate of nickel ions should be the same. The nickel concentration in the reaction solution ought to decrease in theory. We attributed the anomalous increase of nickel concentration to the dissolved of unstable tiny fibrous particles owing to the Ostwald ripening effect. This opinion was further confirmed by continuously pumping ammonia solutions into a nickel oxalate dihydrate suspension. The nickel oxalate dihydrate particles gradually dissolved and were transformed to fibrous morphology in ammonia solutions (Fig. S5a–j, ESI†). In this experiment, nickel concentrations in the reaction solution also increased when large clusters with tiny fibers appeared suggesting the redissolution of small fibers occurred. After the feeding process, the concentration of nickel ion decreased again through the growth of fibrous particles and remained steady after the aging time of 3 h. Compared with the initial solution pH, the pH of reaction solution increased a little and varied in the range of 9.82–9.93 which might be caused by the release of OH^- coordinated with Ni^{2+} in the initial nickel-ammonia solution.

3.5 Single crystal of nickel ammine oxalate

Blue crystals stable in air and water were synthesized under the single crystal experiment. The formula of the blue crystal was $Ni(NH_3)_2C_2O_4$. The elemental analyses gave the following results: found (Ni 15.22 wt%; H 3.29 wt%; C 13.25 wt%), calculated for $C_2H_6N_2NiO_4$ (Ni 15.50 wt%; H 3.32 wt%; C 13.28 wt%). One crystallographically independent nickel atom was coordinated with four oxygen atoms in two oxalate ions and two nitrogen atoms in two ammonia molecules to form an octahedral geometry (Fig. 6a). The crystal belonged to monoclinic system where eight nickel atoms located in the vertexes of unit cell and two nickel atoms existed on the center of front and back surfaces (Fig. 6d). Further details of the X-ray structural analysis and selected bond lengths and angles were given in Table 1 and appendix Table S1 (ESI).†

Compared with the fibrous nickel oxalate synthesized under the typical experiment, there was no crystalline water in the blue crystal. In order to know the structure deviation of $Ni(NH_3)_{1.7}C_2O_4 \cdot 2.2H_2O$ from $Ni(NH_3)_2C_2O_4$, the polycrystalline powders corresponding to the blue crystal were synthesized by rotating the vessel and cooling quickly in the single crystal experiment to destroy the mild growth environment for developing single crystals. The polycrystalline powders with a rod-like morphology also had high aspect ratios and its XRD pattern was similar to the fibrous nickel oxalate at the typical experiment suggesting the coincident crystal structure of $Ni(NH_3)_{1.7}C_2O_4 \cdot 2.2H_2O$ and $Ni(NH_3)_2C_2O_4$ (Fig. 6b and c). The leftmost XRD peak was not the strongest in the polycrystalline powders which might be caused by the insufficient development of rod-like particles. In the crystal unit cell of $Ni(NH_3)_2C_2O_4$, the direction of oxalate chains was parallel to the *b*-axis. The surface energy of crystal plane (020), which was perpendicular to the *b*-axis in the nickel ammine oxalate, might increase greatly due to the existence of ammonia (Fig. 6d). The atomic stacking rate in this crystal plane became faster resulting in crystal growing along the plane's normal direction and the final exposure of crystal plane (200) and (001) which had the two biggest interplanar spacing in $Ni(NH_3)_2C_2O_4$. This was also the reason why the two leftmost peaks had the strongest intensity in the XRD pattern of fibrous nickel oxalate.

Table 1 Crystallographic details for the synthesized blue crystal

Empirical formula	$C_2H_6N_2NiO_4$
Formula weight	180.80
Crystal system	Monoclinic
Space group	*C*2/*m*
a	10.763 Å
b	5.411 Å
c	4.996 Å
β	96.295(6)°
V	289.21(7) $Å^3$
Z	2
Density (calculated)	2.076 g cm^{-3}
F(000)	184
μ	3.296 mm^{-1}
Crystal size	0.240 × 0.220 × 0.200 mm^3
Reflections collected	973
Independent reflections	371 [$R_{(int)} = 0.0078$]
Goodness-of-fit on F^2	1.118
R_1, wR_2 (all data)	0.0140, 0.0362

In summary, amorphous nickel oxalate lump particles started to appear first during the preparation of fibrous nickel oxalate. Then the nitrogen contents in solid products gradually increased since ammonia coordinated with nickel causing the changes of products' crystal structures. In the meanwhile, the products' morphology changed from lump particles to spindle-like clusters, columnar particles, and fibers. Following the LaMer model, the reaction system which had low supersaturation switched to crystal growth stage immediately after primary nucleation during the feeding process. In the aging process, Ostwald ripening occurred: small fibrous particles gradually dissolved and large fibrous particles grew. The products' morphology and crystal structure were almost unchanged after four hours of aging. The fundamental reason for the formation of fibrous nickel oxalate was the existence of ammonia molecules in the (020) crystal plane which might cause the high surface energy of (020), and thus nickel oxalate crystal preferred

to grow along with it (Fig. 6e). These phenomena indicated ligands had great influences on the crystal growth resulting in unexpected product morphology during the preparation of materials by wet chemistry methods.

4 Conclusion

Fibrous nickel oxalate with a formula of $Ni(NH_3)_{1.7}C_2O_4 \cdot 2.2H_2O$ was prepared by the ammonia coordination method. In the feeding process, amorphous nickel oxalate without ammonia in its crystal lattice appeared first. Then ammonia gradually coordinated with nickel atoms, and the solid products changed from lump particles to spindle-like clusters, columnar particles and fibrous particles. In the aging process, Ostwald ripening occurred where small fibrous particles gradually dissolved and large fibrous particles grew. The crystal structure of fibrous nickel oxalate suggested that the fundamental reason for the formation of fibrous nickel oxalate was the existence of ammonia molecules in the (020) crystal plane which might cause the high surface energy of (020), and thus nickel oxalate crystal preferred to grow along with it. This work provides a feasible way to synthesize metallic materials with high aspect ratios and provides examples and references for preparing materials with extraordinary morphology by simple coordination-precipitation methods.

Author contributions

H. Ma: conceptualization, methodology, investigation, data curation, writing-original draft. Z. Y. Liu: data curation, writing-review & editing. Z. H. Liu: conceptualization, resources, writing-review & editing, supervision, data curation.

Conflicts of interest

There are no conflicts to declare.

Acknowledgements

This research was supported by Chongzuo Science and Technology Plan Project (grant number: FA2019016).

References

1 J. Schneider, P. Rohner, D. Thureja, M. Schmid, P. Galliker and D. Poulikakos, Electrohydrodynamic nanodrip printing of high aspect ratio metal grid transparent electrodes, *Adv. Funct. Mater.*, 2016, **26**, 833–840.

2 L. A. Bauer, N. S. Birenbaum and G. J. Meyer, Biological applications of high aspect ratio nanoparticles, *J. Mater. Chem.*, 2004, **14**, 517–526.

3 D. Raciti, T. Braun, B. M. Tackett, H. Xu, M. Cruz, B. J. Wiley and T. P. Moffat, High-aspect-ratio Ag nanowire mat electrodes for electrochemical CO production from CO_2, *ACS Catal.*, 2021, **11**, 11945–11959.

4 A. Das and R. G. Nair, Effect of aspect ratio on photocatalytic performance of hexagonal ZnO nanorods, *J. Alloys Compd.*, 2020, **817**, 153277.

5 Y. X. Tang, Y. Y. Zhang, J. Y. Deng, D. P. Qi, W. R. Leow, J. Q. Wei, S. Y. Yin, Z. L. Dong, R. Yazami, Z. Chen and X. D. Chen, Unravelling the correlation between the aspect ratio of nanotubular structures and their electrochemical performance to achieve high-rate and long-life lithium-ion batteries, *Angew. Chem., Int. Ed.*, 2014, **126**, 13706–13710.

6 T. M. Whitney, J. S. Jiang, P. C. Searson and C. L. Chien, Fabrication and magnetic properties of arrays of metallic nanowires, *Science*, 1993, **261**, 1316–1319.

7 Y. Li, G. W. Meng, L. D. Zhang and F. Phillipp, Ordered semiconductor ZnO nanowire arrays and their photoluminescence properties, *Appl. Phys. Lett.*, 2000, **76**, 2011–2013.

8 Z. Miao, D. S. Xu, J. H. Ouyang, G. L. Guo, X. S. Zhao and Y. Q. Tang, Electrochemically induced sol–gel preparation of single-crystalline TiO_2 nanowires, *Nano Lett.*, 2002, **2**, 717–720.

9 Q. Yang, J. Sha, X. Y. Ma and D. R. Yang, Synthesis of NiO nanowires by a sol–gel process, *Mater. Lett.*, 2005, **59**, 1967–1970.

10 G. B. Ji, S. L. Tang, B. L. Xu, B. X. Gu and Y. W. Du, Synthesis of $CoFe_2O_4$ nanowire arrays by sol–gel template method, *Chem. Phys. Lett.*, 2003, **379**, 484–489.

11 F. J. Douglas, D. A. MacLaren, C. Renero-Lecuna, R. D. Peacock, R. Valiente and M. Murrie, Self-assembly of ultra-thin lanthanide oxide nanowires *via* surfactant-mediated imperfect oriented attachment of nanoparticles, *CrystEngComm*, 2012, **14**, 7110–7114.

12 Y. Xing, M. Li, S. A. Davis and S. Mann, Synthesis and characterization of cerium phosphate nanowires in microemulsion reaction media, *J. Phys. Chem. B*, 2006, **110**, 1111–1113.

13 Q. Huang, L. L. Chai, X. Wang, Y. L. Wu, Q. P. Li, Y. Hu and J. J. Qian, Co/N-doped carbon nanosheets derived from InOF-1 precursors for efficient Zn–air battery, *Microporous Mesoporous Mater.*, 2021, **314**, 110868.

14 Q. Huang, Y. Y. Guo, D. D. Chen, L. J. Zhang, T. T. Li, Y. Hu, J. J. Qian and S. M. Huang, Rational construction of ultrafine noble metals onto carbon nanoribbons with efficient oxygen reduction in practical alkaline fuel cell, *Chem. Eng. J.*, 2021, **424**, 130336.

15 W. Chern, K. Hsu, I. S. Chun, B. P. de Azeredo, N. Ahmed, K. H. Kim, J. M. Zuo, N. Fang, P. Ferreira and X. L. Li, Nonlithographic patterning and metal-assisted chemical etching for manufacturing of tunable light-emitting silicon nanowire arrays, *Nano Lett.*, 2010, **10**, 1582–1588.

16 X. L. Li, Metal assisted chemical etching for high aspect ratio nanostructures: a review of characteristics and applications in photovoltaics, *Curr. Opin. Solid State Mater. Sci.*, 2012, **16**, 71–81.

17 Z. R. Smith, R. L. Smith and S. D. Collins, Mechanism of nanowire formation in metal assisted chemical etching, *Electrochim. Acta*, 2013, **92**, 139–147.

18 F. J. Wendisch, M. Abazari, H. Mahdavi, M. Rey, N. Vogel, M. Musso, O. Diwald and G. R. Bourret, Morphology-graded silicon nanowire arrays *via* chemical etching: engineering optical properties at the nanoscale and

macroscale, *ACS Appl. Mater. Interfaces*, 2020, **12**, 13140–13147.
19 T. Okamoto, R. Ichino, M. Okido, Z. H. Liu and C. F. Zhang, Effect of ammonia on the crystal morphology of nickel oxalate precipitates and their thermal decomposition into metallic nickel, *Mater. Trans.*, 2005, **46**, 171–174.
20 C. F. Zhang, J. Zhan, J. H. Wu and C. J. Li, Preparation and characterization of fibrous NiO particles by thermal decomposition of nickelous complex precursors, *Trans. Nonferrous Met. Soc. China*, 2004, **14**, 713–717.
21 C. F. Zhang, J. Zhan, J. H. Wu, X. Y. Guo and M. Okido, Preparation of fibrous nickel oxide particles, *Trans. Nonferrous Met. Soc. China*, 2003, **13**, 1440–1445.
22 Z. Y. Liu, Z. H. Liu, Q. H. Li, T. Z. Yang and D. M. Zhang, Formation mechanism of fibrous cobalt oxalate precipitated from alkaline Co^{2+}–NH_3–$C_2O_4^{2-}$–H_2O system, *Mater. Chem. Phys.*, 2011, **131**, 102–107.
23 Y. L. Yao, C. F. Zhang, Y. Q. Fan and J. Zhan, Preparation and microwave absorbing property of porous FeNi powders, *Adv. Powder Technol.*, 2016, **27**, 2285–2290.
24 J. Zhan, D. F. Zhou and C. F. Zhang, Shape-controlled synthesis of novel precursor for fibrous Ni–Co alloy powders, *Trans. Nonferrous Met. Soc. China*, 2011, **21**, 544–551.
25 J. Zhan, Y. Yao, C. F. Zhang and C. J. Li, Synthesis and microwave absorbing properties of quasione-dimensional mesoporous $NiCo_2O_4$ nanostructure, *J. Alloys Compd.*, 2014, **585**, 240–244.
26 Y. Q. Fan, C. F. Zhang, J. h. Wu, J. Zhan and P. Yang, Composition and morphology of complicated copper oxalate powder, *Trans. Nonferrous Met. Soc. China*, 2010, **20**, 165–170.
27 C. F. Zhang, Y. L. Yao, Y. L. Zhang and J. Zhan, Preparation of ultra-fine fibrous Fe–Ni alloy powder by coordinated co-precipitation-direct reduction process, *Trans. Nonferrous Met. Soc. China*, 2012, **22**, 2972–2978.
28 J. Zhan, Z. L. Miao, M. Cai and Q. H. Li, Boosting ethanol oxidation over nickel oxide through construction of quasi-one-dimensional morphology and hierarchically porous structure, *Trans. Nonferrous Met. Soc. China*, 2020, **30**, 1615–1624.
29 N. Jongen, P. Bowen, J. Lemaître, J. Valmalette and H. Hofmann, Precipitation of self-organized copper oxalate polycrystalline particles in the presence of hydroxypropylmethylcellulose (HPMC): control of morphology, *J. Colloid Interface Sci.*, 2000, **226**, 189–198.
30 K. S. Weil, The synthesis of transition metal nitrides *via* thermolysis of metal–ammine complexes, part I: chromium nitride, *J. Solid State Chem.*, 2008, **181**, 199–210.
31 R. L. Frost, J. Yang and Z. Ding, Raman and FTIR spectroscopy of natural oxalates: implications for the evidence of life on Mars, *Chin. Sci. Bull.*, 2003, **48**, 1844–1852.
32 S. Chenakin and N. Kruse, Thermal decomposition of nickel oxalate dihydrate: a detailed XPS insight, *J. Phys. Chem. C*, 2019, **123**, 30926–30936.
33 J. Zhan, Y. H. He, D. F. Zhou and C. F. Zhang, Thermodynamic analysis on synthesis of fibrous Ni–Co alloys precursor and Ni/Co ratio control, *Trans. Nonferrous Met. Soc. China*, 2011, **21**, 1141–1148.
34 J. Zarzycki, M. Prassas and J. Phalippou, Synthesis of glasses from gels: the problem of monolithic gels, *J. Mater. Sci.*, 1982, **17**, 3371–3379.
35 D. Horn and J. Rieger, Organic nanoparticles in the aqueous phase–theory, experiment, and use, *Angew. Chem., Int. Ed.*, 2001, **40**, 4330–4361.